fire

MDPI

Article

Analyzing Fire Severity and Post-Fire Vegetation Recovery in the Temperate Andes Using Earth Observation Data

Melanie Maxwald [1,2,*], Markus Immitzer [3], Hans Peter Rauch [2] and Federico Preti [1,4]

[1] Dipartimento di Scienze e Tecnologie Agrarie, Alimentari, Ambientali e Forestali (DAGRI), Università degli Studi di Firenze, 50144 Firenze, Italy
[2] Department of Civil Engineering and Natural Hazards, Institute of Soil Bioengineering and Landscape Construction (IBLB), University of Natural Resources and Life Sciences, Vienna (BOKU), Peter-Jordan-Straße 82, 1190 Vienna, Austria
[3] Department of Landscape, Spatial and Infrastructure Sciences, Institute of Geomatics, University of Natural Resources and Life Sciences, Vienna (BOKU), Peter-Jordan-Straße 82, 1190 Vienna, Austria
[4] AIPIN (Soil and Water Bioengineering Italian Association), Via di San Bonaventura 13, 50145 Firenze, Italy
* Correspondence: melanie.maxwald@boku.ac.at

Abstract: In wildfire areas, earth observation data is used for the development of fire-severity maps or vegetation recovery to select post-fire measures for erosion control and revegetation. Appropriate vegetation indices for post-fire monitoring vary with vegetation type and climate zone. This study aimed to select the best vegetation indices for post-fire vegetation monitoring using remote sensing and classification methods for the temperate zone in southern Ecuador, as well as to analyze the vegetation's development in different fire severity classes after a wildfire in September 2019. Random forest classification models were calculated using the fire severity classes (from the Relativized Burn Ratio—*RBR*) as a dependent variable and 23 multitemporal vegetation indices from 10 Sentinel-2 scenes as descriptive variables. The best vegetation indices to monitor post-fire vegetation recovery in the temperate Andes were found to be the Leaf Chlorophyll Content Index (LCCI) and the Normalized Difference Red-Edge and SWIR2 (NDRESWIR). In the first post-fire year, the vegetation had already recovered to a great extent due to vegetation types with a short life cycle (seasonal grass-species). Increasing index values correlated strongly with increasing fire severity class (fire severity class vs. median LCCI: 0.9997; fire severity class vs. median NDRESWIR: 0.9874). After one year, the vegetations' vitality in low severity and moderate high severity appeared to be at pre-fire level.

Keywords: wildfire; remote sensing; Sentinel-2; fire severity; vegetation indices; random forest; vegetation recovery; northern South America

Citation: Maxwald, M.; Immitzer, M.; Rauch, H.P.; Preti, F. Analyzing Fire Severity and Post-Fire Vegetation Recovery in the Temperate Andes Using Earth Observation Data. *Fire* **2022**, *5*, 211. https://doi.org/10.3390/fire5060211

Academic Editors: Guilherme Mataveli, Gabriel de Oliveira, Renata Libonati, Liana Anderson and Celso H. L. Silva-Junior

Received: 21 October 2022
Accepted: 5 December 2022
Published: 8 December 2022

1. Introduction

While the analysis of the fourth-generation global fire emission database (GFED4) [1], between the years 2000 and 2012, shows a modest decrease in global wildfire incidences, the amount of burned areas in most environments increased, whereby the most affected ecosystems were savannahs, open shrubland and subtropical grasslands. Climate change and the resulting extreme weather events, such as droughts, influence the intensity of fires. In total, 13.3 million individual fires, globally, were reported by the Global Fire Atlas between 2003 and 2016 [2]. The estimated direct average carbon emission into the atmosphere from the burned biomass between 1997 and 2016 was 2.2×10^{15} g of carbon per year (Pg C yr^{-1}) [3], whereby the process of decay of the burned trunks in some regions indirectly releases further emissions years after the wildfire event [4]. Supporting measures for the fast recovery of the vegetation after a wildfire are therefore important to bind CO_2 from the atmosphere, and several authors have conducted work on this topic [5–8]. The fire severity (FS) is an important indicator regarding the post-fire vitality of the affected vegetation, as well as probable necessary supportive measures for recovery. Space Agencies,

such as NASA [4] and ESA (Copernicus program with two equal satellites—Sentinel 2A and 2B) [9], document the wildfire phenomena around the planet with earth observation data. They deliver an important and open access base to elaborate remotely sensed information regarding FS, as well as the recovery of vegetation. In many affected areas, the increase in the intensity of the fires decreases the ability to resprout, as the soil seed banks are diminished during the wildfire [10], or vegetation parts at the subsurface, such as rhizomes, are damaged by the heat. The required time of the vegetations' recovery depends on the vegetation type itself and differs strongly between forest areas and grassland due to their different life cycles. Certain weed species found in some fire prone areas, particularly in Savannahs, are adapted to frequent wildfires and are therefore stimulated positively by heat and smoke [11], and some even require fire to geminate [12]. FS is therefore an important parameter when assessing the impact of a wildfire on vegetation. For the definition of the FS through earth observation data, the differenced Normalized Burn Ratio (*dNBR*) [13] derived from pre- and post-fire satellite imagery, as well as the Relativized Burn Ratio (*RBR*) [14] in cases of areas with low or sparse vegetation before the fire event [15], are frequently used spectral indices. They aim to determine the extent of the wildfire area, as well as the degree of change in vegetation caused by the fire [13]. Further, the mentioned burn ratios help to immediately identify fire effects, as well as to assess vegetative recovery potential and delayed mortality during the following growing season [13]. However, follow-up monitoring of vegetation recovery in post-fire years is usually undertaken using vegetation indices (VI), such as the Normalized Difference Vegetation Index (NDVI) [16], or the Soil Adjusted Vegetation Index (SAVI) [17], etc., calculated from multitemporal satellite scenes from the affected area over a number of years. These VIs map the vitality of the vegetation and serve municipalities, planning parties or forest management institutions to classify and define the development or stadium to which extent the burnt area recovered, and maintenance steps can be evaluated accordingly. The maintenance of fire prone areas to support vegetation recovery after wildfires can speed up the recovery process of the vegetation by up to 10 years [18]; however, accurate measures differ according to region, climate, as well as vegetation composition, and are therefore an important topic to work on [5]. Various investigations address the vegetation's recovery after wildfires in the Mediterranean area [19,20], northern America [8,21,22], Siberia [23], as well as Australia [24]. Further studies were developed for the humid tropics [5], as well as the Páramo region [25–27], the latter covering areas in northern South America from Venezuela, Colombia, Ecuador, and Peru. In Ecuador, scientific studies have been conducted using remote sensing methods e.g., modeling and simulation of wildfires next to urban areas [28], forest fire susceptibility monitoring using machine learning techniques [29], as well as fire severity effects on physical-chemical soil properties in southern Ecuador [30]. To the current knowledge of the authors, scientific publications defining the best VIs for the monitoring of vegetation recovery in post-fire conditions are not existent. Moreover, studies investigating the correlation between FS and vegetation recovery in the temperate climate (no dry season, warm summer—Cfb, Köppen-Geiger-Classification) in southern Ecuador were not found. The Loja province is covered by various climate zones, which leads to different combinations of vegetation and different needs when developing effective restoration methods after wildfires. Therefore, further studies are required to better understand and predict the responses of vegetation to fire, as well as to define the restoration measures necessary in the area. As already mentioned, VIs derived from remote sensing methods are a useful and open access tool to better understand the post-fire vegetation recovery. However, the choice to use an appropriate VI for vegetation recovery monitoring depends on the vegetation composition and climate zone of the area in question, as different VIs provide different levels of sensitivity for grassland, canopy moisture or plant structures [31]. For post-fire vegetation recovery monitoring using VIs, the correlation to FS is an important aspect, as it strongly influences the regrowth rate. The present study investigates the best VIs for fire prone areas at the Cfb climate zone in southern Ecuador using random forest classification models. Furthermore, the autonomous vegetation recovery capacity

is assessed using remote sensing techniques by analyzing a fire event which occurred in September 2019 in the canton Quilanga. The results can support municipalities or planning parties to better understand the vegetation's behavior in post-fire conditions, as well as to estimate whether recuperating measures are necessary at the area in question.

The primary objectives of the present investigation were:

- To elaborate the FS of the fire event in September 2019 at the El Saco basin.
- To identify the most appropriate VIs derived from Sentinel-2 (S2) images for the monitoring of vegetation recovery after wildfires in the temperate climate zone in southern Ecuador.
- To assess the vegetation recovery in the different FS classes based on the previous selection of the best VIs for post-fire monitoring at the area in question.

2. Materials and Methods

2.1. Study Site

The investigated wildfire area is located in a mountainous, temperate zone (Cfb) in the southern Andes (Sierra) of Ecuador in the canton Quilanga, which is part of the province of Loja on the Peru border. It is characterized by grass- and shrub-land, as well as some forest patches with non-native tree species, such as pine or eucalyptus, which tend to dry out the soil and therefore influence the development of native vegetation. Further, coffee production, farming and pastureland characterize the landscape. In the area of concern, the precipitation value is approximately 1100 mm per year, whereby the months from December to April/May are characterized by intense rain events [32]. From June to November, the risk of fires increases due to the decline in precipitation; in recent years, three intense wildfires have been reported: in 2012 (Parroquia Fundochamba, sector Collingora, Quilanga); 2016 (Parroquia Fundochamba, sector Guaguasaco, Quilanga); and the investigated event, in 2019 [33]. The last wildfire, caused by farmers intending to prepare farmland in the beginning of September 2019, affected more than 8000 ha and lasted for more than two weeks (Figure 10). For the present study, the basin of the river El Saco (Figure 1), with a linear distance of 2500 m southeast from the center of Quilanga to the outflow point, was chosen. It covers an area of 984.3 ha, reaches from 1520 m at the outflow point to 2680 m a.s.l. at the highest point and includes one main and two micro basins; the length of the mainstream is 4.83 km. Table 1 shows the different climate zones in Loja/Ecuador according to the Köppen-Geiger-Classification.

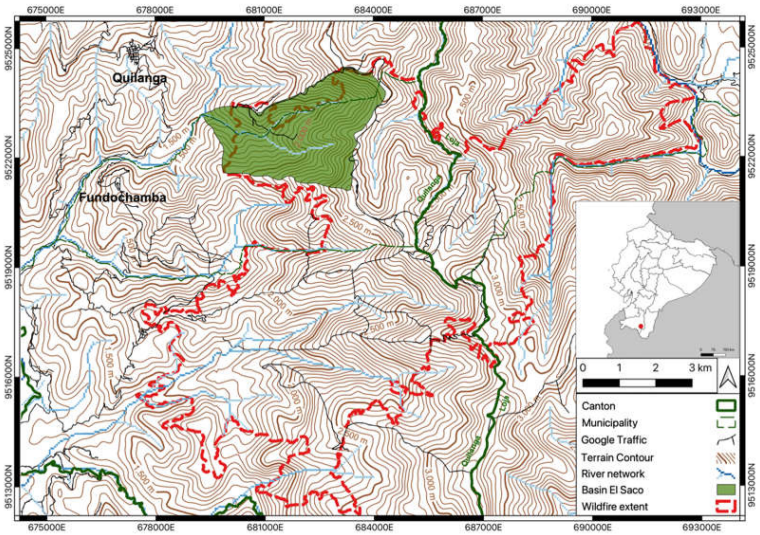

Figure 1. Location and extent of the wildfire area (red), as well as the river El Saco basin (green) in Quilanga, Ecuador; Background: contour map of elevation and river network derived from DEMs (credit: Marc Souris, IRD), Road network: Google Traffic.

Table 1. Climate zones in Loja (Ecuador), according to Köppen-Geiger-Classification.

Climate Zones in the Province of Loja	
Aw	Tropical, savannah
BSh	Arid, steppe, hot
BWh	Arid, desert, hot
Cfb	Temperate, no dry season, warm summer
Cfc	Temperate, no dry season, cold summer
Csb	Temperate, dry summer, warm summer
Cwb	Temperate, dry winter, warm summer
ET	Polar, tundra

2.2. Workflow

The investigation of the wildfire area in this temperate zone of southern Ecuador is based on various elaborations from the data, gained remotely (Figure 2). In the first step the *RBR*, the FS was calculated, providing the basis for further evaluation. The second step consisted of the identification of the best VIs for the monitoring of vegetation recovery in the study area. In total, 23 VIs (Appendix A, Table A1) were calculated from atmospherically corrected, multitemporal S2 scenes (Level 2A products). In addition, random forest classification models (with feature selection) describing the FS class were set up for every used S2 scene at the El Saco basin to identify the most influencing VIs within the models. In the third step, the selected VIs were used for the analysis of the post-fire vegetation recovery within the different FS classes.

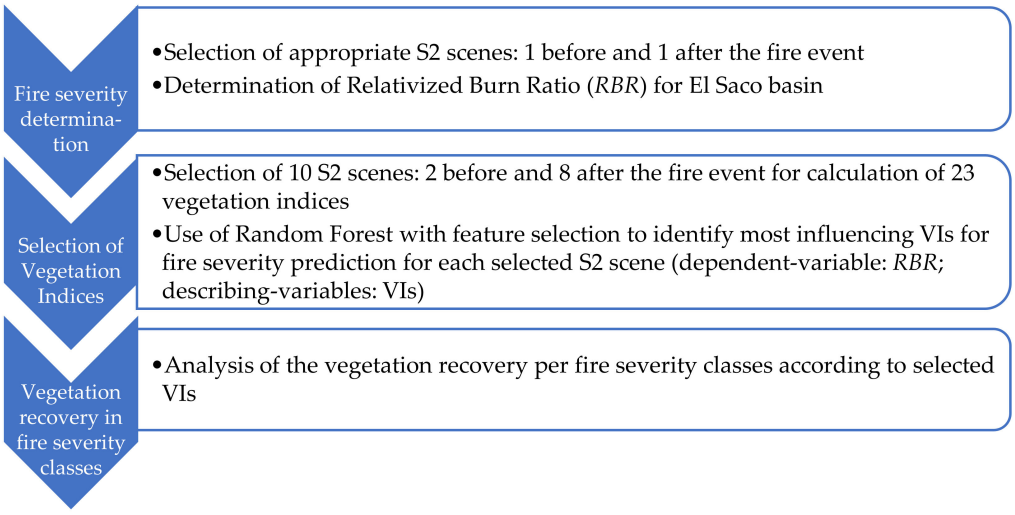

Figure 2. Workflow of the analysis of vegetation recovery at each fire severity class in the temperate (Cfb) zone in northern South America.

2.2.1. Elaboration of the Fire Severity

For the present investigation, the FS was assessed and remotely sensed from S2 images with a spatial resolution of 10 m. Atmospherically corrected S2 images (Level 2A products), taken on 31 July 2019 and 29 September 2019, were selected for the evaluation, considering the cloud coverage at the time of the recordings above the El Saco basin. In the first step, the *NBR* [34] was calculated for both images using the freely accessible SNAP program. Furthermore, the *dNBR* between the two scenes, as well as the *RBR* (Equation (1) [15]), were calculated.

$$RBR = \left(\frac{dNBR}{\left(NBR_{pre-fire} + 1001 \right)} \right) = \left(\frac{NBR_{pre-fire} - NBR_{post-fire}}{\left(NBR_{pre-fire} + 1001 \right)} \right) \quad (1)$$

A water and cloud mask of the images was created with the help of the *NDWI* (Equation (2) [15]) as water bodies can have a similar *NBR* difference.

$$NDWI = \frac{Green - NIR}{Green + NIR} = \frac{B3 - B8}{B3 + B8} \quad (2)$$

As the absolute *dNBR* may misclassify pixels in areas with little vegetation before the fire event and because the first image of the El Saco basin was captured during the season with less precipitation, the *RBR* was chosen for further usage in the following models. After exporting the calculated *RBR* image as a GeoTIFF file, the pixels were classified in QGIS, based on fire intensity (Table 2). The higher the value in a pixel, the lower the vitality of the vegetation in that location.

Table 2. Classification of the fire severity from the Relativized Burn Ratio according to United States Geological Survey—USGS [35].

Classification	*RBR*-Value
High regrowth	−0.500 to −0.251
Low regrowth	−0.250 to −0.101
Unburned	−0.100 to 0.099
Low severity	0.100 to 0.269
Moderate low severity	0.270 to 0.439
Moderate high severity	0.440 to 0.659
High severity	0.660 to 1.300

2.2.2. Identification of the Best VIs for the Monitoring of Vegetation Recovery in Different Fire Severity Classes

In the study area, no supporting post-fire measures regarding vegetation or erosion protection were carried out by the municipality. Therefore, the natural recovery capacity of the vegetation located at the El Saco basin, without anthropogenic influence, within the first two years after the fire event, could be analyzed. Ten atmospherically corrected Level 2A products (two before and eight after the fire event) of the S2A and S2B platform were chosen, taking into consideration cloud coverage and the change of vegetation in the area over a year. From the eight scenes chosen after the fire event, two scenes were selected within the first two months after the fire event (Nr. 3, 4; Table 3) to monitor the short-term development of the vegetation. Moreover, three scenes were chosen for each of the following years (2020: Nr.5–7 and 2021: Nr.8–10; Table 3), starting from the end of the rainy season (April/May) until one and two years after the fire event.

Table 3. Summary of selected Sentinel-2 scenes; Granule: T17MPR.

Nr.	Sentinel-2 Satellite	Date	Sun Zenith Angle	Sun Azimuth Angle
1	A	6 June 2019	35.06	39.19
2	B	31 July 2019	33.31	47.13
		Fire Event		
3	B	29 September 2019	21.12	86.18
4	B	18 November 2019	24.54	129.68
5	A	21 April 2020	28.19	54.44
6	A	10 June 2020	35.50	38.95
7	B	24 August 2020	28.19	57.90
8	A	26 May 2021	33.78	40.46
9	A	5 July 2021	36.06	40.83
10	A	3 September 2021	25.91	63.91

Spectral indices derived from satellite images are widely used to map burned areas [36–38], as well as to monitor the vegetation's development after a fire event [23,37,39,40]. For this study,

23 VIs (Appendix A, Table A1) were calculated for every S2 scene and databases were created by extracting the VI-values according to the FS class (unburned, low severity, moderate low severity, moderate high severity) derived from the *RBR* at the El Saco basin. To determine the best VIs for the vegetation monitoring at the study area, a pixel-based classification was carried out using the Random Forest approach, after Breiman [41], with the FS class from the *RBR* (classified after USGS [35]) as the dependent variable. This approach is frequently used for FS mapping [16], as well as for the classification of vegetation or tree species [42]. For this study, the parameter *mtry* (number of predictors samples randomly for each node) was taken as the square root of the number of input parameters and *ntree* (number of trees) was set to 500 at each classification (default values). In addition, a recursive feature selection process was applied using the mean decrease in accuracy (MDA), which is used to measure the performance of the model without a specific describing variable. The removal of a variable with a high MDA value would cause the model to lose accuracy in prediction. The higher the MDA value, the higher the importance of the variable to the accuracy of the model. Further, the results of the classification models were assessed by the out of bag (OOB) error [42]. The classification of the FS class with feature selection was run with every database containing the data of the VIs of every S2-scene. The BEST model (according to the overall accuracy (OA)) was chosen to be representative for the respective date. The variables (=VIs) of these BEST models were checked regarding matching VIs between the different dates to obtain a preselection of VIs. To prove that these matching VIs are suitable for post-fire vegetation monitoring in the temperate Andes, new databases were set up for model calculation at each date, containing the FS class as the dependent variable and the matching VIs as the describing variables. Further, four additional databases were set up for the scenes of the years: (I) 2020; (II) 2021; (III) eight scenes (not using the scenes nr. 2 and 3, which were part of the *RBR* calculation); and (IV) all ten scenes containing the FS class as the dependent variable and the matching VIs as the describing variables. With these 10 single-date and four multi-date databases, the Random Forest classification of the FS class was repeated and the two best performing VIs in these models were used to analyze the vegetation development in the FS classes. Figure 3 illustrates the identification process of the best VIs for the monitoring of the post fire vegetation recovery.

2.2.3. Analysis of Vegetation Recovery in Different Fire Severity Classes

The vegetation recovery in the different FS classes at the El Saco basin was studied using boxplot diagrams, descriptive statistics, and time series. The VIs selected in the previous step were analyzed at one pre- and three post-fire moments from 2018 to 2021, (around the month of the fire event, with a maximum difference of two months due to cloud coverage) to understand the post-fire development of the vegetation at the El Saco basin in the different FS classes. Further, the delta of the VIs for the first, the second, and the first two post-fire years was calculated and statistically analyzed. While the analysis of the VIs' delta shows the recovery at each FS class within the first and the second post-fire year, another important question was whether the pre-fire level of the vegetation's vitality could be obtained again according to the VIs. As it was not possible to obtain cloud free S2 scenes from the El Saco basin for the same month over four years (2018–2021), the median values at the unburned area were used as reference values to understand the phenological change, which influenced the post-fire images. The pre-fire medians of the VI values at each FS class were set to a reference level of 100% and the difference in the following years was calculated as percentage points [PP].

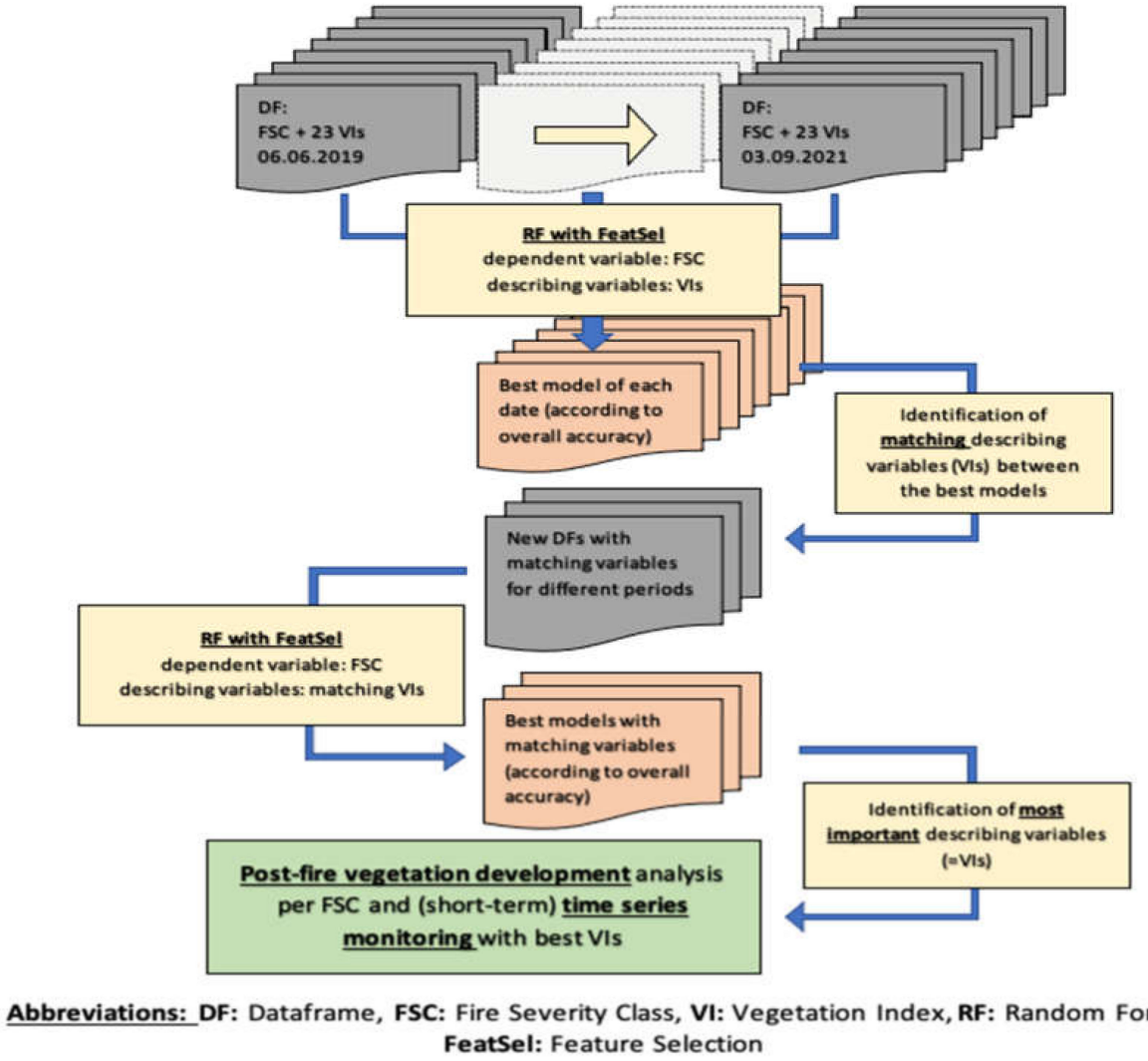

Figure 3. Identification of vegetation indices for post-fire vegetation development analysis per fire severity class and time series monitoring in the temperate Andes.

3. Results

3.1. Elaboration of the Fire Severity

The FS elaborated from S2 images with the formula of the *RBR* is shown in Figure 4a,c. From the total size of the El Saco basin (984.30 ha), 781.25 ha and, therefore, 79.37% were affected by the fire event. In the northeastern part of the basin, 0.07% and 0.30% of the pixels were classified as "high regrowth" and "low regrowth". These fragments can be defined as misinterpretation as the calculated water and cloud mask (*NDWI*) did not cover some parts of the cloud shadows and thus led to this misclassification. The class "unburned" (UB) covers 4.54% and was classified mainly along the river courses of the basin. Further, "low severity" (LS) was determined at 18.82% of the pixels. The biggest part of the area was classified as "moderate low severity" (MLS), with 54.74%, and the class "moderate high severity" (MHS) achieved 21.38%. The maximum FS class "high severity" (HS) was classified at 0.15% of the burned area in the El Saco basin (Figure 4b). With the exception of the mentioned misclassification due to cloud shadows, the field investigation mostly confirmed the FS map. The vegetation in areas with HS or MHS showed the complete destruction of the biomass on the surface. MLS or LS were classified in areas where higher vegetation, such as shrubs or trees, were burned at the base with intact, green parts on the crown, as well as in areas of the grassland, where some ferns and grass species sprouted again one month after the fire event.

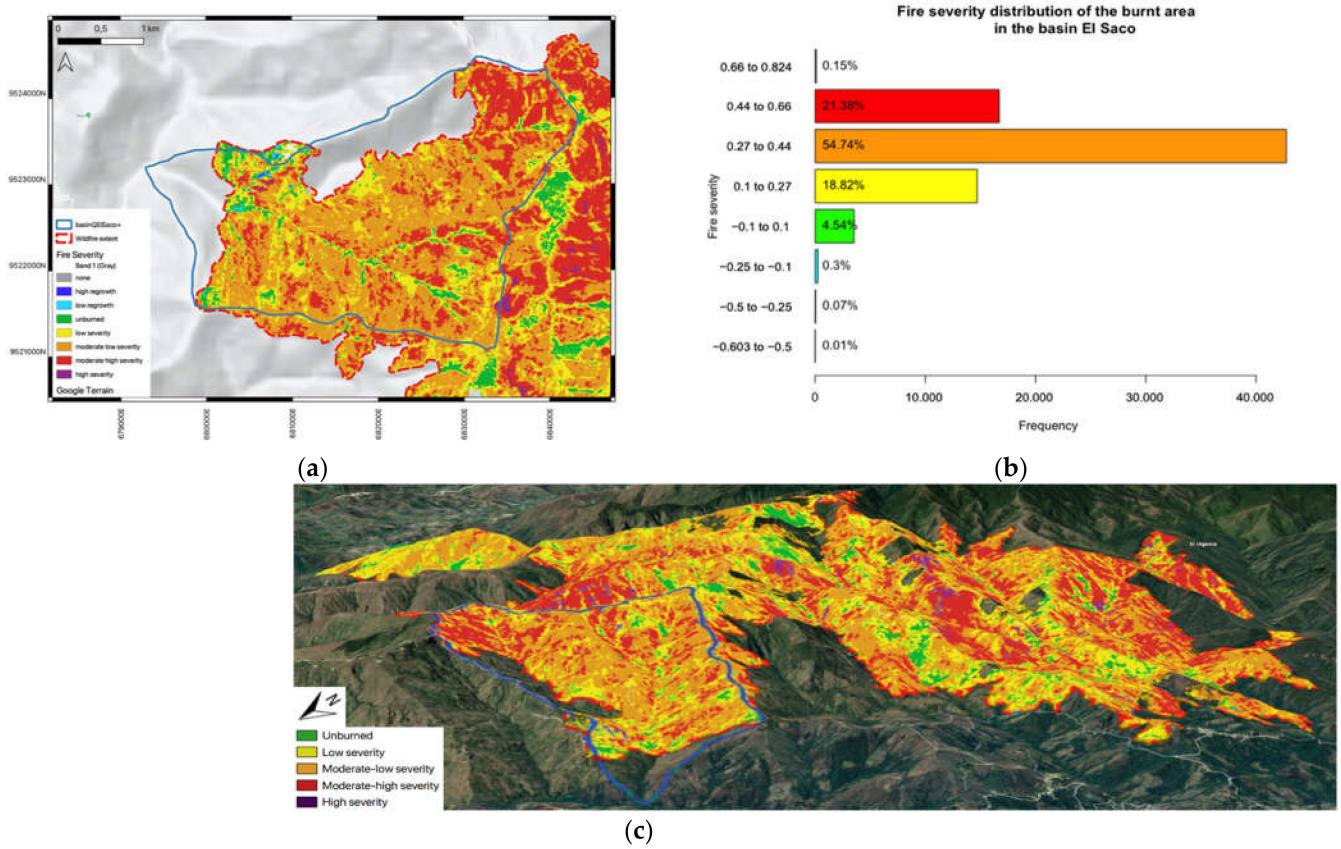

Figure 4. (**a**) Fire severity after the wildfire in September 2019 at the El Saco basin, canton Quilanga/Ecuador. Base map: Google Terrain; (**b**) Distribution of the fire severity within the burnt area of El Saco at the canton Quilanga/Ecuador after the wildfire in September 2019; (**c**) Overview of the wildfire area 2019 from the viewpoint Quilanga in Google Earth Pro.

3.2. Identification of the Best VIs for Post-Fire Monitoring in the Temperate Andes

To identify the best VIs for the monitoring of the vegetation recovery at each FS class, ten BEST simple models using the VIs of each date were calculated (Table 4). The OA resulted between 57.8% and 84.9%, with a median of 63.4%. The most significant model predicting the *RBR* was the one of 29 September 2019 (84.9%), two weeks after the wildfire. This can be explained as this scene was used for the *RBR* calculation, as well as the low time lag from the fire event. The OA of the two scenes before the fire event is around 67% and the worst classified model derives from the S2-scene on 10 June 2020 (OA 57.8%). From the three S2-scenes in 2020 and 2021, the ones at the end of the rainy season achieved an OA of 67.7% and 63.1%, respectively. The number of variables for each BEST model differs due to the applied feature selection function. Therefore, the occurrence of the same Vis in the different BEST models was checked. As a result, the Leaf Chlorophyll Content Index (LCCI), the Normalized Difference Red-Edge and SWIR2 (NDRESWIR), as well as the Red Edge Peak Area (REPA), were part of every model.

To verify that these matching VIs were suitable for post-fire vegetation monitoring at the area in question, new databases were set up containing only LCCI, NDRESWIR and REPA. As a result, the OA ranged between 75.0% and 81.3%, with a median of 76.8%, for these models (Table 5); a minimum increase of 7.8% and a maximum increase of 17.3% in OA compared to the BEST models appeared. The model from September 29, 2019, again showed the highest OA, but decreased by 3.6% compared to the BEST model. While the model from this date achieved 81.3% in OA with the three descriptive variables LCCI, NDRESWIR and REPA, the BEST model used 12 VIs as descriptive variables to achieve an OA of 84.9%.

Table 4. BEST Random Forest models based on OOB results after Feature Selection using 23 Vegetation Indices from single Sentinel-2 data recording dates.

BEST MODELS: Dependent Variable: *RBR*; Descriptive Variables: 23 Vegetation Indices Classification: Random Forest with Feature Selection					
Scene Nr:	**S2 Acquisition Date**	***n* Variables after Feature Selection**	**Split**	**Overall Accuracy**	**Kappa**
1	6 June 2019	4	2	67.1%	0.503
2	31 July 2019	4	2	67.5%	0.508
Fire Event					
3	29 September 2019	12	3	84.9%	0.779
4	18 November 2019	9	3	63.7%	0.444
5	21 April 2020	4	2	67.7%	0.511
6	10 June 2020	6	2	57.8%	0.342
7	24 August 2020	5	2	61.4%	0.408
8	26 May 2021	5	2	63.1%	0.436
9	5 July 2021	5	2	60.6%	0.401
10	3 September 2021	7	2	60.0%	0.383
Result: LCCI, NDRESWIR, REPA were part of every BEST model					

Table 5. Random Forest models using three Vegetation Indices (LCCI, NDRESWIR, REPA) from single Sentinel-2 data recording dates.

MODELS: Dependent Variable: *RBR*; Descriptive Variables: LCCI, NDRESWIR, REPA Classification: Random Forest						
Scene Nr:	**S2 Acquisition Date**	***n* Variables**	**Split**	**Overall Accuracy**	**Change in Accuracy Compared to BEST Models**	**Kappa**
1	6 June 2019	3	1	75.5%	+8.4%	0.636
2	31 July 2019	3	1	75.3%	+7.8%	0.634
Fire Event						
3	29 September 2019	3	1	81.3%	−3.6%	0.725
4	18 November 2019	3	1	76.6%	+12.9%	0.654
5	21 April 2020	3	1	77.0%	+9.3%	0.660
6	10 June 2020	3	1	75.0%	+17.2%	0.628
7	24 August 2020	3	1	76.9%	+15.5%	0.660
8	26 May 2021	3	1	77.0%	+13.9%	0.661
9	5 July 2021	3	1	76.4%	+15.8%	0.651
10	3 September 2021	3	1	77.3%	+17.3%	0.666

The additional model calculations from the databases containing the VIs for the S2-scenes in 2020, 2021, as well as combinations of eight and all ten scenes, helped to understand the change in OA where multitemporal Sentinel scenes were used (Table 6). The best combined models from both individual years showed an OA of approximately 82% using all nine input variables. The model derived from the eight S2 scenes (without the scenes from *RBR* calculation) showed an OA of 83.5%, using 22 variables (of 24). The best combined model from all ten scenes and, therefore, with the ones used for the *RBR* calculation, resulted with an OA of 86.3% (eleven input variables). According to the

MDA of the combined models, the most important input variables were the LCCI and the NDRESWIR. These VIs were used for the monitoring of the vegetation recovery.

Table 6. Best Random Forest models based on OOB results after Feature Selection using three Vegetation Indices (LCCI, NDRESWIR, REPA) from different Sentinel-2 data recording series.

BEST MODELS: Dependent Variable: *RBR*; Descriptive Variables: LCCI, NDRESWIR, REPA Classification: Random Forest with Feature Selection						
Scene Nr:	Vegetation Indices from Different S2 Scenes	*n* Variables after Feature Selection	Split	Overall Accuracy	Kappa	3 Most Influencing Variables According to Mean Decrease Accuracy
5–7	LCCI, NDRESWIR, REPA 3 SC 2020	9	3	82.4%	0.744	LCCI 24 August 2020 NDRESWIR 21 April 2020 LCCI 21 April 2020
8–10	LCCI, NDRESWIR, REPA 3 SC 2021	9	3	82.6%	0.746	LCCI 03 September 2021 LCCI 26 May 2021 NDRESWIR 3 September 2021
1 and 4–10	LCCI, NDRESWIR, REPA 8 SC 2019 to 2021 (no scenes from *RBR* calculation)	22	4	83.5%	0.760	NDRESWIR 21 April 2020 LCCI 18 November 2019 LCCI 26 May 2021
1–10	LCCI, NDRESWIR, REPA 10 SC 2019 to 2021 (with scenes from *RBR* calculation)	11	3	86.3%	0.800	NDRESWIR 31 July 2019 NDRESWIR 29 September 2019 REPA 29 September 2019

3.3. Analysis of the Vegetation Recovery in Different Fire Severity Classes

3.3.1. LCCI and NDRESWIR in One Pre- and Three Post-Fire Scenes

Immediately after the fire event, the two analyzed VIs showed that with the increasing FS class, the lower and the upper quartiles converged, and the median decreased (Appendix A: Tables A2 and A3; Figures 5 and 6). At the VIs from the S2 scene of 24 August 2020, about one year after the fire event, the medians in all four FS classes were higher compared to the pre-fire year; thus, the time difference of two months (August and October) and the phenological development due to the rainy season from December to May must be considered (Section 3.3.3.). Figures 5 and 6 show the boxplots of the VI values per FS class in the different years.

3.3.2. Development of the LCCI and the NDRESWIR in the First Two Post-Fire Years

When analyzing the vegetation's development using the delta of the VIs between post-fire scenes, the median values showed a high positive correlation with increasing FS classes in the first year (LCCI: 0.9997, NDRESWIR: 0.9874). At the MHS area, the recuperation appeared to be the highest, followed by MLS and LS (Figures 7 and 8). The second post-fire year showed continuously equilibrated, slightly decreasing median dLCCI, as well as dNDRESWIR values with increasing FS. The vegetation at the study area seemed to be recuperating strongly in the first post-fire year.

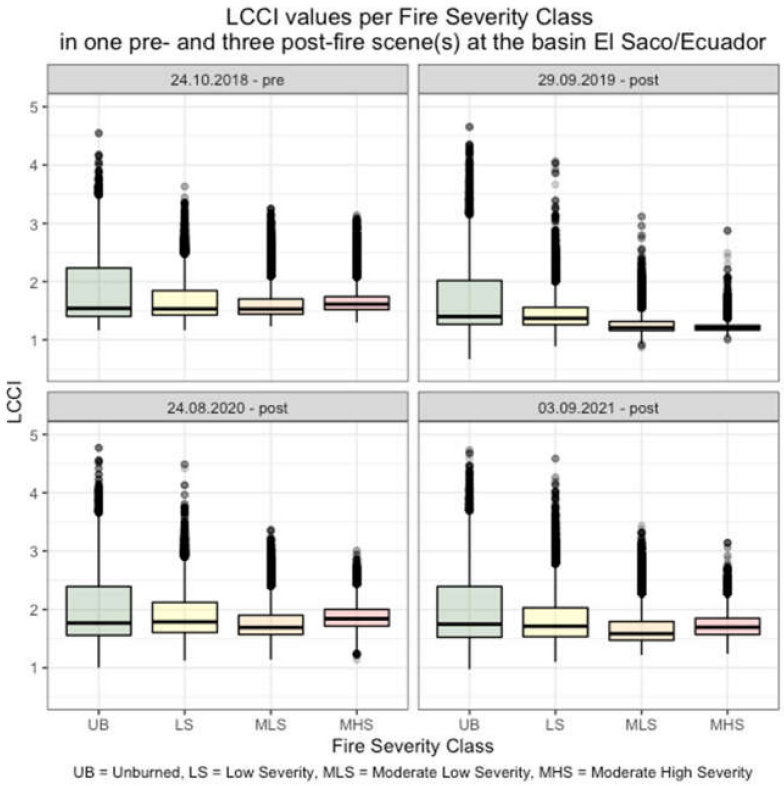

Figure 5. Boxplots of LCCI values in the fire severity classes at the El Saco basin in one pre- and three post-fire Sentinel 2 scenes.

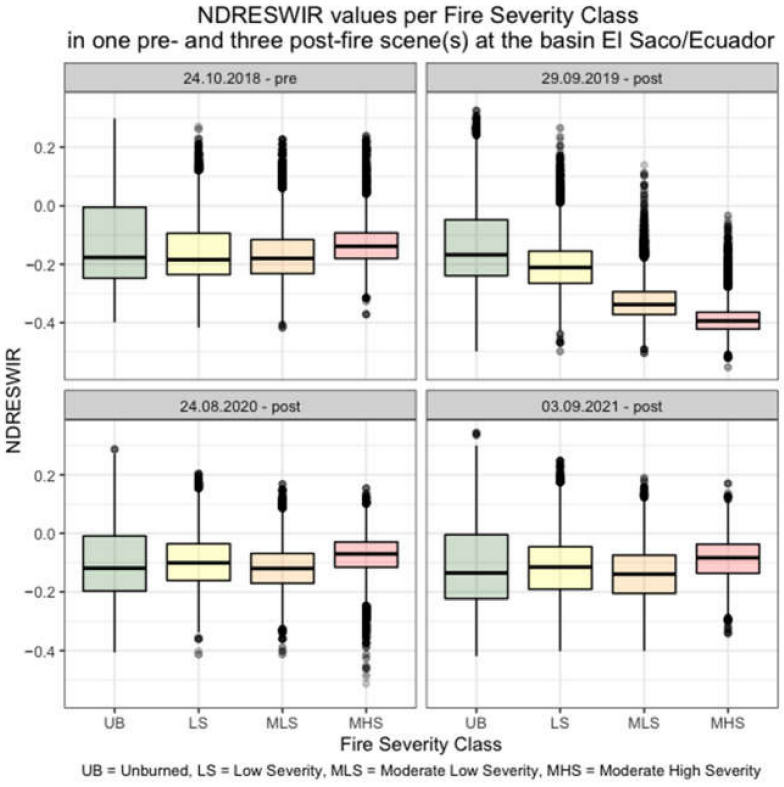

Figure 6. Boxplots of NDRESWIR values in the fire severity classes at the El Saco basin in one pre- and three post-fire Sentinel 2 scenes.

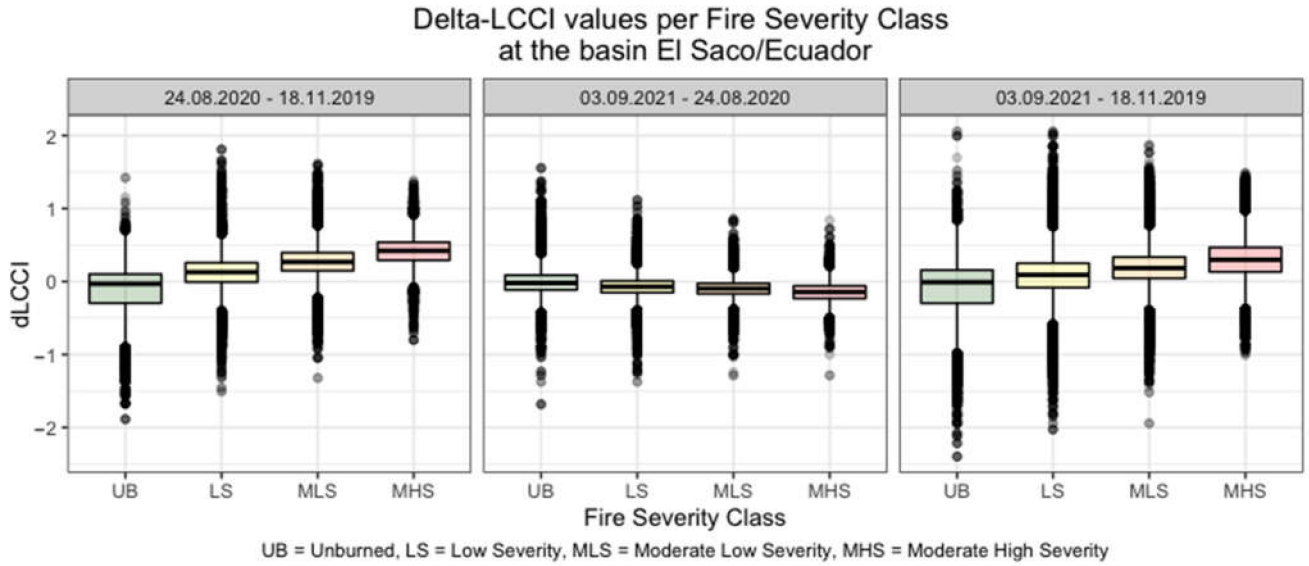

Figure 7. Boxplots of dLCCI values per fire severity classes from the first two post-fire years at the El Saco basin.

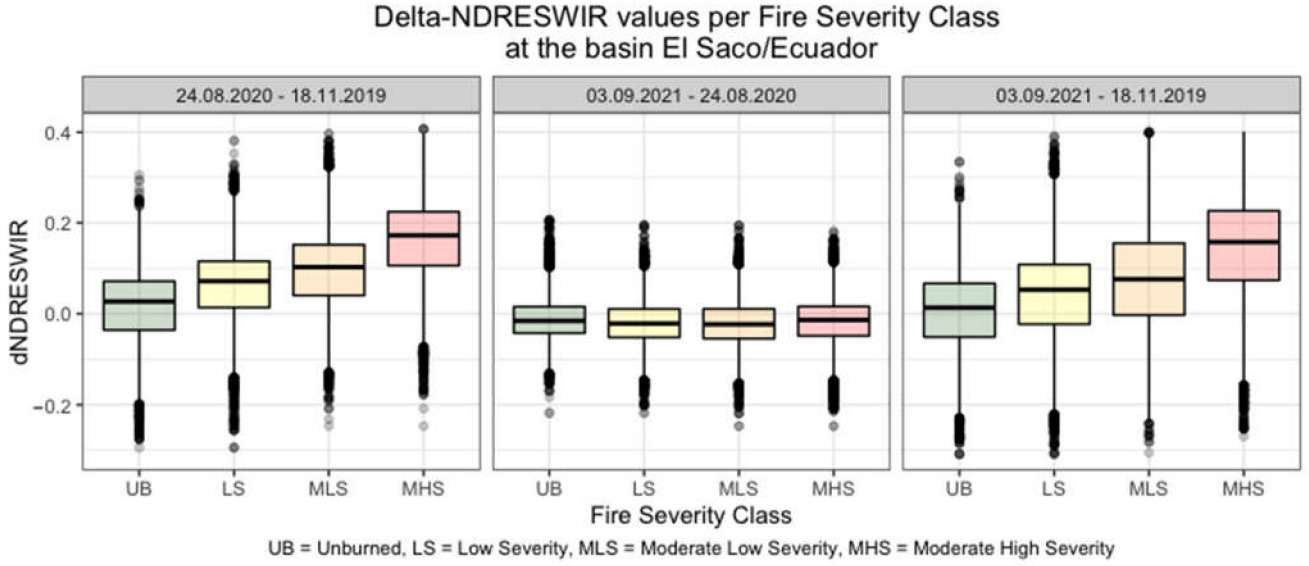

Figure 8. Boxplots of dNDRESWIR values per fire severity classes from the first two post-fire years at the El Saco basin.

3.3.3. Relative Post-Fire Development of LCCI and NDRESWIR Per Fire Severity Class

Due to the different acquisition times of the S2 images (cloud-free data), which were used for the analysis of the vegetation's post-fire development, the UB area served as a reference to understand the relative change of the median within the FS classes. Comparing the two post-fire years with the pre-fire year 2018 showed that the LCCI median in the UB area in 2020 was +14.87 PP higher. due to the two months of difference with the pre-fire scene, and caused by the different influence of the phenology (Table 7). The chosen S2 scene in 2021 had a similar LCCI median value in the UB area (+13.57 PP) compared to the pre-fire year in 2018. The NDRESWIR median in the UB area, showing a +32.76 PP of relative increase in 2020 and +23.72 PP in 2021 related to pre-fire conditions (Table 8). When relativizing the time difference, the LCCI showed an increase in 2020 of +1.92 PP at the area with LS, a decrease of −4.00 PP at the MLS, as well as a decrease of −0.54 PP at the MHS compared to the pre-fire image in 2018 (Table 9). According to the LCCI, the vegetation in LS and the MHS areas recovered one year after the fire event to about the same level as was

measured in the pre-fire conditions in 2018. In the second post-fire year, the LCCI indicated a decrease in all FS classes, whereby the MLS again showed the lowest value, with −9.71 PP. Interpreting the relativized data from the NDRESWIR (Table 10), the LS and MHS areas performed better compared with MLS, whereby all three FS classes were at least around the same level as the pre-fire year in 2018.

Table 7. Vegetation recovery according to the median LCCI per fire severity class compared to the pre-fire year in percentage points (PP) at the El Saco basin.

Change of LCCI Median with Year and Fire Severity				
	Pre-Fire 24 October 2018	**Post-Fire 29 September 2019**	**Post-Fire 24 August 2020**	**Post-Fire 3 September 2021**
Unburned	100.00 PP	−9.09 PP	+14.87 PP	+13.57 PP
Low severity	100.00 PP	−10.58 PP	+16.79 PP	+11.95 PP
Moderate low severity	100.00 PP	−20.96 PP	+10.87 PP	+3.86 PP
Moderate high severity	100.00 PP	−25.62 PP	+14.33 PP	+5.27 PP

Table 8. Vegetation recovery according to the median NDRESWIR per fire severity class compared to the pre-fire year in percentage points (PP) at the El Saco basin.

Change of NDRESWIR Median with Year and Fire Severity				
	Pre-Fire 24 October 2018	**Post-Fire 29 September 2019**	**Post-Fire 24 August 2020**	**Post-Fire 3 September 2021**
Unburned	100.00 PP	+5.08 PP	+32.76 PP	+23.72 PP
Low severity	100.00 PP	−14.05 PP	+45.41 PP	+37.84 PP
Moderate low severity	100.00 PP	−87.78 PP	+33.33 PP	+22.78 PP
Moderate high severity	100.00 PP	−185.51 PP	+49.28 PP	+39.13 PP

Table 9. LCCI time series: relativizing the phenological difference of the selected vegetation index dates at the El Saco basin.

Relativized Change of LCCI Median			
	Post-Fire 29 September 2019	**Post-Fire 24 August 2020**	**Post-Fire 3 September 2021**
Unburned	0.00 PP	0.00 PP	0.00 PP
Low severity	−1.49 PP	+1.92 PP	−1.62 PP
Moderate low severity	−11.87 PP	−4.00 PP	−9.71 PP
Moderate high severity	−16.53 PP	−0.54 PP	−8.30 PP

Table 10. NDRESWIR time series: relativizing the phenological difference of the selected vegetation index dates at the El Saco basin.

Relativized Change of NDRESWIR MEDIAN			
	Post-Fire 29 September 2019	**Post-Fire 24 August 2020**	**Post-Fire 3 September 2021**
Unburned	0.00 PP	0.00 PP	0.00 PP
Low severity	−19.13 PP	+12.65 PP	+14.12 PP
Moderate low severity	−92.86 PP	+0.57 PP	−0.94 PP
Moderate high severity	−190.59 PP	+16.52 PP	+15.41 PP

The calculated PP cannot be compared directly between the two selected VIs, as they refer to different benchmarks, derived from different S2 bands and formulas. Nevertheless, both VIs show a similar, V-shaped trend (Figure 9), as the LS and MHS have a higher relative increase than the MLS area when comparing it with pre-fire conditions.

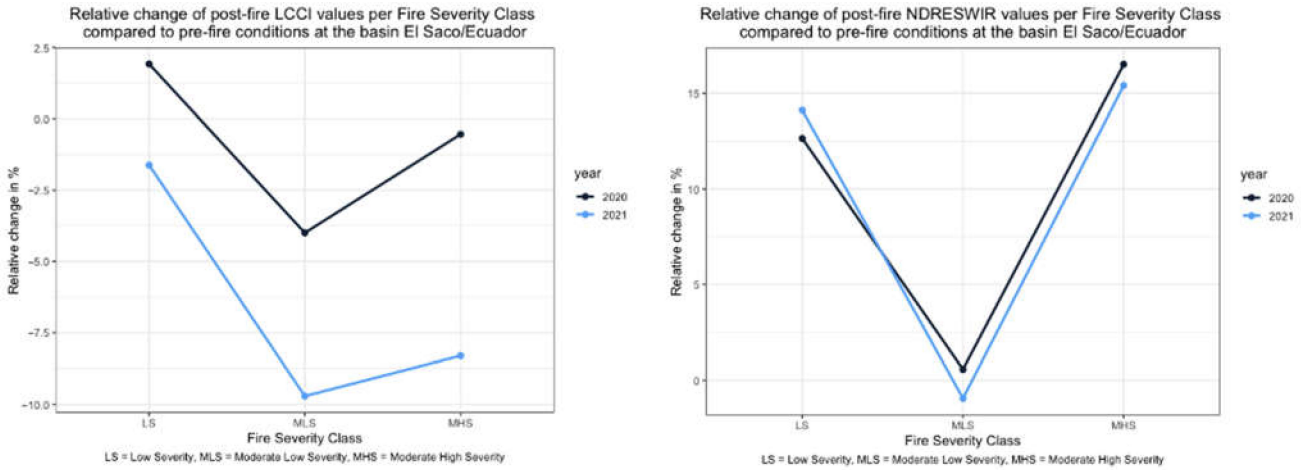

Figure 9. Relative change of post-fire vegetation index values per fire severity class compared to pre-fire conditions at the El Saco basin.

4. Discussion

When classifying the FS using Random Forest for every single scene of the used dates, before and after the fire event, widely used VIs for time series monitoring, such NDVI, or Soil Adjusted Vegetation Index (SAVI) [8,40,43,44], were not part of the final models. The *NBR*, which is frequently used for post-fire vegetation monitoring [22], was part of one model (29 September 2019), which questions the application of this index for grassland-dominated areas. The understanding that the optimal spectral or VIs for quantifying FS depends on vegetation composition or forest type is reported in different studies [24,34,45]. Tran et al. (2018) [24] considers the different spectral indices for FS assessment; namely, NDVI, *NBR*, Normalized Difference Water Index (NDWI), Normalized Difference Vegetation Index Thermal (NDVIT), Normalized Burn Ratio Thermal (NBRT), Vegetation Index 6 Thermal (VI6T), Burned Area Index (BAI), Modified Soil Adjusted Vegetation Index (MSAVI), Mid InfraRed Burn Index (MIRBI) and Char Soil Index (CSI). While the best performing VI for open forests with mixed fire responses (resprouters and seeders) in the Australian temperate forests was the dNDVI, the most accurate VI for obligate seeder closed forests was found to be the delta Normalized Difference Water Index (dNDWI) [24]. In 2001, Trigg and Flasse [46] developed the Mid-Infrared Burn Index (MIRBI) for savannahs, using the short wavelength and long-wavelength mid-infrared bands from MODIS. A further study, assessing VIs for post-fire vegetation recovery monitoring in grass- and/or shrubland was found in China/Mongolia by Qin et al. (2021), who recommended the Normalized Difference Phenology Index (NDPI) [47]. One problem when comparing these studies is that there are numerous VIs from different sources (Sentinel, Landsat, MODIS, etc. [47,48]), with different recording conditions, as well as different temporal and spatial resolution. This fact leads to a certain variance between the central wavelengths of the input bands and, therefore, to probable deviations in the calculated VIs. Another problem is that there is some ambiguity regarding the abbreviations of spectral and VIs used in scientific studies. For example, BAI is short for Burned Area Index [49], but also for Built-up Area Index [50]. The authors therefore recommend strongly to report used formulas, as well as names, when using VIs. Globally, with the increasing number of open access earth observation data, the remote sensing of fire events is gaining increasing attention. Numerous VIs are being developed or revised [51,52]; leading, on one hand, to more accurate tools, but on the other hand, to probable oversupply and user confusion. In addition, when assessing different VIs for the specific use in certain areas, it can be challenging to cover all important aspects for post-fire monitoring. However, this study presents a scalable methodology to assess VIs for post-fire vegetation recovery monitoring, applicable on other vegetation and climate conditions, using also additional VIs. Compared to other reported studies, the number of VIs examined (n = 23) in this paper is relatively high. The importance of LCCI,

NDRESWIR and REPA to monitor vegetation recovery after wildfires in the temperate zone in southern Ecuador, with sparse tree vegetation and broad grassland, was shown as they conclude to FS class prediction. The RED, all RED EDGE, as well as the NEAR INFRARED (SHORTWAVE INFRARED) bands of the S2 satellite images, contributed to the post-fire vegetation development analysis in this study. This result should be considered in future studies when monitoring vegetation recovery in former wildfire areas in the temperate zone (Cfb), as well as areas with similar vegetation types. The vegetation recovery analysis in the different FS classes showed that within the first two years, the vegetation recovered to a great extent. In particular, the grassland recovered fully within the first post-fire year, which coincides with a study from Li and Guo (2018) in a North American mixed prairie [44]. At the El Saco basin, areas with higher severity and, therefore, a higher incision in the vegetation, developed faster in post-fire conditions. Nevertheless, LS and MHS seemed to recover better, equalizing or surpassing the pre-fire level within the first post-fire year. This is most likely due to the release of nutrients, which changes with fire severity [53]. The time of vegetation recovery varies with different biomes. Therefore, the recovery period required in forests and riparian vegetation types to regrow to pre-fire conditions is higher compared to grasslands and steppe areas, where fires potentially increase the amount of biomass [54]. Asrar et al. (1989) [55] stated that burned prairie grassland showed higher leaf production in burned areas. Further studies showed that more severely damaged areas recover faster after the fire event than areas with lower severity [54,56]. As vegetation monitoring with satellite data provides information regarding the amount of biomass, or the leaf area at the location, one important note is that the present analysis does not specify the type of vegetation if no reference data is given. In some cases, it could therefore be possible that the values of the VIs may be higher than before the fire event, leading to a better evaluation of the situation as it is. Some densely growing ferns, which are facilitated by fires or pioneer vegetation, could be the reason for higher VI values, indicating good recovery in areas where trees are burned, for which recuperation time is higher due to a longer life cycle and therefore slower growth compared to pioneer vegetation. One possible solution could be to use multitemporal S2 scenes with reference data regarding the vegetation types at the area in question to classify the vegetation [42] and acquire information regarding the development of vegetation types or species after the wildfire. This implies, further, that the classification model of the vegetation type depends on monitoring in the field or the exact interpretation of orthophotos. While short-term monitoring can be sufficient for grass- or shrub-land, higher growing vegetation with a longer recuperation time will not be covered within two years.

(**a**) (**b**)

Figure 10. (**a**) Fire-affected shrub and tree vegetation layer (**b**) Impact of the wildfire on the landscape one month after the event in the canton Quilanga/Ecuador [57].

Globally, the effects of wildfires are receiving increasing attention with the increasing number of extreme weather events and droughts. Being able to estimate the numerous consequences can help to diminish and minimize post-fire effects on landscapes, ecosystems, and/or settlements. Post-fire vegetation monitoring with adequate VIs from satellite data, according to climate zone and vegetation type, can help planning parties to assess these effects properly and determine suitable measures. When implementing post-fire measures using soil and water bioengineering techniques to revegetate or mitigate erosion [57–59], the use of time series from VIs can help to understand where to place the measures, spatially, at the area in question. Knowing from experience, or from post-fire monitoring with satellite data, that, for example, the vegetation in high severity areas recovers fast, can help planning parties to decide whether to apply measures in the area or not. The financial and time effort for planning and applying post-fire measures can be made more effective by using remote sensing data and VIs. However, in addition to monitoring or recuperation strategies for vegetation, educational work could have a high impact on the prevention of fire events and, therefore, the preservation of an intact vegetation cover. As farmers in the area use fire frequently (traditional slash and burn method [60]) to remove vegetation from the surface of their land to prepare it for seeding [61], days with a high risk of wildfires during the season with less precipitation should be avoided. Most of the residents have access to internet with their smartphones. Therefore, the development and promotion of an application such as the Fire Weather Index (FWI) [62], tuned for the area in question, showing the daily wildfire risk due to various meteorological variables, such as air temperature, relative humidity, wind speed and total precipitation, could help to prevent the spreading of uncontrolled fire events. Further, the extension of infrastructure for fire departments could have a high impact towards successfully limiting the spread of wildfires.

5. Conclusions

This study showed that for the monitoring of the post-fire vegetation recovery with sparse tree vegetation and broad grassland in the temperate Andes (Cfb), LCCI, as well as NDRESWIR, were the best VIs. Widely used VIs such as NDVI or SAVI were not part of the calculated final models. It underlines the assumption that the VI used for the monitoring of post-fire vegetation development should be selected according to the main vegetation type. As VIs do not indicate the vegetation type, there is no information regarding the development of specific species at the area in question. The short-term monitoring (<2 years) of vegetation recovery can be sufficient for grassland but must be extended for several years in areas with higher vegetation, such as shrubs or trees. According to vegetation monitoring with the selected VIs, the plants' recovery showed a strong positive correlation with the increasing FS class within the first two post-fire years at the investigated area. A repetition of the study within the following years may provide further information regarding the recovery of different vegetation types. Possible restauration strategies for the area should refer to the vegetation recovery, combining remote sensing methods with as field monitoring. By providing these answers to the research questions, a solid basis for possible landscape and forest restoration strategies after wildfires in the temperate (Cfb) zone in northern South America is delivered and the need for supporting or revegetating interventions can be evaluated. Municipalities or planning parties can use this information as a basis to develop further post-fire recuperation strategies. According to the knowledge of the authors, to date, no such study has been carried out for the temperate zone in southern Ecuador. The result of the present investigation is therefore an important contribution to recovering landscapes after fires in this region.

Author Contributions: Conceptualization, M.M. and H.P.R.; methodology, M.M. and M.I.; investigation, M.M.; writing—original draft preparation, M.M.; writing—review and editing, M.M., M.I., H.P.R. and F.P.; visualization, M.M.; supervision, H.P.R. and F.P.; funding acquisition, F.P. All authors have read and agreed to the published version of the manuscript.

Funding: This study was financially supported by Consorzio di Bonifica Basso Valdarno and Erasmus+ (UNIFI Italy and UPS Ecuador).

Informed Consent Statement: Not applicable.

Data Availability Statement: Not applicable.

Acknowledgments: Special thanks go to Giulio Castelli, Cristiano Foderi and Giovanni Mastrolonardo (University of Florence), as well as Michael de Latour for their input to improving the manuscript. Further thanks go to Edwin Mario Japón Abad and Ronald Correa for their warm welcome and help in the field, as well as the municipality of Quilanga for providing information regarding the study site.

Conflicts of Interest: The authors declare that they have no known competing financial interest or personal relationships that could have appeared to influence the work reported in this paper.

Appendix A

Table A1. Formulas used for the calculation of the vegetation indices using Sentinel-2 scenes from the wildfire area in Quilanga/Ecuador.

Nr.	Name	Formula	Source
1	Built-up Area Index (BAI)	$\frac{BLUE-NIR}{BLUE+NIR}$	[50]
2	Chlorophyll Green index (CGI)	$\frac{NIR}{GREEN+RE1}$	[63]
3	Global Environmental Monitoring Index (GEMI)	$\eta - 0.25\eta^2 - \frac{RED-0.125}{1-RED}$ $\eta = \frac{2(NIR^2-RED^2)+1.5NIR+0.5RED}{NIR+RED+0.5}$	[64]
4	Greenness Index (GI)	$\frac{GREEN}{RED}$	[65]
5	Green Normalized Difference Vegetation Index (gNDVI)	$\frac{NIR-GREEN}{NIR+GREEN}$	[66]
6	Leaf Chlorophyll Content Index (LCCI)	$\frac{RE3}{RE1}$	[67]
7	Normalized Difference Red-Edge and SWIR2 (NDRESWIR)	$\frac{RE2-SWIR2}{RE2+SWIR2}$	[68]
8	Normalized Difference Vegetation Index (NDVI)	$\frac{NIR-RED}{NIR+RED}$	[69]
9	Red-Edge Normalized Difference Vegetation Index (reNDVI)	$\frac{NIR-RE1}{NIR+RE1}$	[66]
10	Normalized Burn Ratio (NBR)	$\frac{NIR-SWIR2}{NIR+SWIR2}$	[13,15]
11	Red-Edge Peak Area (REPA)	$RED + RE1 + RE2 + RE3 + NIR$	[68,70]
12	Red-Edge Triangular Vegetation Index (RETVI)	$100(NIR - RE1) - 10(NIR - GREEN)$	[71]
13	Soil Adjusted Vegetation Index (SAVI)	$\frac{NIR-RED}{NIR+RED+0.5}1.5$	[17]
14	Blue and RE1 ratio (SRBRE1)	$\frac{BLUE}{RE1}$	[65]
15	Blue and RE2 ratio (SRBRE2)	$\frac{BLUE}{RE2}$	[72]
16	Blue and RE3 ratio (SRBRE3)	$\frac{BLUE}{RE3}$	[68]
17	NIR and Blue ratio (SRNIRB)	$\frac{NIR}{BLUE}$	[73]
18	NIR and Green ratio (SRNIRG)	$\frac{NIR}{GREEN}$	[65]
19	NIR and Red ratio (SRNIRR)	$\frac{NIR}{RED}$	[73]
20	NIR and RE1 ratio (SRNIRRE1)	$\frac{NIR}{RED1}$	[63]
21	NIR and RE2 ratio (SRNIRRE2)	$\frac{NIR}{RED2}$	[68]
22	NIR and RE3 ratio (SRNIRRE3)	$\frac{NIR}{RED3}$	[68]
23	Water Body Index (WBI)	$\frac{BLUE-RED}{BLUE+RED}$	[74]

Table A2. Statistics of pre- and post-fire LCCI in different fire severity classes at the El Saco basin.

LCCI								
		Min	**Median**	**Mean**	**Max**	**Standard Deviation**	**Skewness**	**Kurtosis**
24.October 2018	UB	1.165	1.540	1.860	4.546	0.615	1.210	3.437
	LS	1.165	1.531	1.684	3.629	0.365	1.463	4.642
	MLS	1.232	1.527	1.613	3.257	0.262	1.938	7.757
	MHS	1.298	1.612	1.672	3.141	0.245	2.283	10.032
29.September 2019	UB	0.668	1.400	1.700	5.244	0.650	1.434	4.641
	LS	0.887	1.369	1.456	4.072	0.314	1.761	7.854
	MLS	0.867	1.207	1.261	3.124	0.157	2.306	12.066
	MHS	0.993	1.199	1.225	2.876	0.103	3.809	33.201
24.August 2020	UB	1.002	1.769	2.024	5.751	0.623	1.228	4.058
	LS	1.124	1.788	1.911	4.487	0.425	1.228	4.377
	MLS	1.141	1.693	1.774	3.369	0.292	1.392	5.250
	MHS	1.141	1.843	1.880	3.007	0.230	0.840	3.953
3.September 2021	UB	0.978	1.749	2.024	6.069	0.674	1.283	4.184
	LS	1.100	1.714	1.841	4.585	0.435	1.454	5.423
	MLS	1.222	1.586	1.678	3.437	0.290	1.613	5.920
	MHS	1.240	1.697	1.733	3.140	0.216	1.129	5.065

Table A3. Statistics of pre- and post-fire NDRESWIR in different fire severity classes at the El Saco basin.

NDRESWIR								
		Min	**Median**	**Mean**	**Max**	**Standard Deviation**	**Skewness**	**Kurtosis**
24 October 2018	UB	−0.398	−0.177	−0.125	0.298	0.153	0.663	2.267
	LS	−0.417	−0.185	−0.158	0.271	0.112	0.760	3.008
	MLS	−0.417	−0.180	−0.168	0.227	0.088	0.760	3.687
	MHS	−0.373	−0.138	−0.132	0.238	0.078	0.975	5.448
29 September 2019	UB	−0.498	−0.168	−0.134	0.325	0.141	0.807	2.969
	LS	−0.498	−0.211	−0.204	0.265	0.090	0.643	3.880
	MLS	−0.504	−0.338	−0.327	0.139	0.066	1.101	5.119
	MHS	−0.553	−0.394	−0.389	−0.033	0.054	1.329	7.360
24 August 2020	UB	−0.406	−0.119	−0.098	0.287	0.126	0.459	2.479
	LS	−0.413	−0.101	−0.097	0.205	0.093	0.204	2.763
	MLS	−0.413	−0.120	−0.118	0.168	0.075	0.179	2.899
	MHS	−0.513	−0.070	−0.075	0.154	0.071	−0.548	4.371
3 September 2021	UB	−0.419	−0.135	−0.105	0.344	0.147	0.576	2.491
	LS	−0.402	−0.115	−0.115	0.248	0.111	0.190	2.815
	MLS	−0.401	−0.139	−0.137	0.190	0.092	0.194	2.683
	MHS	−0.344	−0.084	−0.087	0.170	0.072	−0.139	2.909

References

1. Giglio, L.; Randerson, J.T.; van der Werf, G.R. Analysis of Daily, Monthly, and Annual Burned Area Using the Fourth-Generation Global Fire Emissions Database (GFED4). *J. Geophys. Res. Biogeosci.* **2013**, *118*, 317–328. [CrossRef]
2. Andela, N.; Morton, D.C.; Giglio, L.; Paugam, R.; Chen, Y.; Hantson, S.; van der Werf, G.R.; Randerson, J.T. The Global Fire Atlas of Individual Fire Size, Duration, Speed and Direction. *Earth Syst. Sci. Data* **2019**, *11*, 529–552. [CrossRef]
3. van der Werf, G.R.; Randerson, J.T.; Giglio, L.; van Leeuwen, T.T.; Chen, Y.; Rogers, B.M.; Mu, M.; van Marle, M.J.E.; Morton, D.C.; Collatz, G.J.; et al. Global Fire Emissions Estimates during 1997–2016. *Earth Syst. Sci. Data* **2017**, *9*, 697–720. [CrossRef]
4. NASA's Jet Propulsion Laboratory Satellite Data Record Shows Climate Change's Impact on Fires. Available online: https://climate.nasa.gov/news/2912/satellite-data-record-shows-climate-changes-impact-on-fires/ (accessed on 30 September 2021).

5. Scheper, A.C.; Verweij, P.A.; van Kuijk, M. Post-Fire Forest Restoration in the Humid Tropics: A Synthesis of Available Strategies and Knowledge Gaps for Effective Restoration. *Sci. Total Environ.* **2021**, *771*, 144647. [CrossRef]
6. Rodrigues, M.; Ibarra, P.; Echeverría, M.; Pérez-Cabello, F.; de la Riva, J. A Method for Regional-Scale Assessment of Vegetation Recovery Time after High-Severity Wildfires: Case Study of Spain. *Prog. Phys. Geogr.* **2014**, *38*, 556–575. [CrossRef]
7. Shive, K.L.; Sieg, C.H.; Fulé, P.Z. Pre-Wildfire Management Treatments Interact with Fire Severity to Have Lasting Effects on Post-Wildfire Vegetation Response. *For. Ecol. Manag.* **2013**, *297*, 75–83. [CrossRef]
8. van Leeuwen, W.J.D. Monitoring the Effects of Forest Restoration Treatments on Post-Fire Vegetation Recovery with MODIS Multitemporal Data. *Sensors* **2008**, *8*, 2017–2042. [CrossRef]
9. European Space Agency. European Union Copernicus Open Access Hub. Available online: https://scihub.copernicus.eu/twiki/do/view/SciHubWebPortal/TermsConditions (accessed on 30 September 2021).
10. Maia, P.; Pausas, J.G.; Arcenegui, V.; Guerrero, C.; Pérez-Bejarano, A.; Mataix-Solera, J.; Varela, M.E.T.; Fernandes, I.; Pedrosa, E.T.; Keizer, J.J. Wildfire Effects on the Soil Seed Bank of a Maritime Pine Stand—The Importance of Fire Severity. *Geoderma* **2012**, *191*, 80–88. [CrossRef]
11. Davies, R.J.P.; Whalen, M.A.; Mackay, D.A.; Taylor, D.; Pisanu, P. Does Soil Seed Bank Diversity Limit Post-Fire Regeneration in Small, Fragmented, Long-Unburnt Remnants of Fire Adapted Vegetation? *Biol. Conserv.* **2013**, *158*, 287–295. [CrossRef]
12. Vallejo, V.R.; Arianoutsou, M.; Moreira, F. Fire Ecology and Post-Fire Restoration Approaches in Southern European Forest Types. In *Post-Fire Management and Restoration of Southern European Forests*; Moreira, F., Arianoutsou, M., Corona, P., de las Heras, J., Eds.; Springer: Dordrecht, The Netherlands, 2012; Volume 24, pp. 93–119. ISBN 978-94-007-2207-1.
13. Key, C.H.; Benson, N.C. Landscape Assessment (LA) Sampling and Analysis Methods. In *FIREMON: Fire Effects Monitoring and Inventory System*; Lutes, D.C., Keane, R.E., Caratti, J.F., Key, C.H., Benson, N.C., Sutherland, S., Gangi, L.J., Eds.; Rocky Mountain Research Station, U.S. Department of Agriculture, Forest Service: Fort Collins, CO, USA, 2006; pp. LA 1–LA 55.
14. Parks, S.A.; Dillon, G.K.; Miller, C. A New Metric for Quantifying Burn Severity: The Relativized Burn Ratio. *Remote Sens.* **2014**, *6*, 1827–1844. [CrossRef]
15. RUS Copernicus Burned Area Mapping with Sentinel-2 Using SNAP. Available online: https://rus-copernicus.eu/portal/wp-content/uploads/library/education/training/HAZA02_BurnedArea_Portugal_Tutorial.pdf (accessed on 4 December 2022).
16. Collins, L.; Griffioen, P.; Newell, G.; Mellor, A. The Utility of Random Forests for Wildfire Severity Mapping. *Remote Sens. Environ.* **2018**, *216*, 374–384. [CrossRef]
17. Huete, A.R. A Soil-Adjusted Vegetation Index (SAVI). *Remote Sens. Environ.* **1988**, *25*, 295–309. [CrossRef]
18. Wohlgemuth, T.; Wasem, U.; Hester, C. Waldverjüngung nach Feuer—Konkurrenzstarke Lärche. *Bündnerwald* **2010**, *63*, 28–33.
19. Gemitzi, A.; Koutsias, N. Assessment of Properties of Vegetation Phenology in Fire-Affected Areas from 2000 to 2015 in the Peloponnese, Greece. *Remote Sens. Appl.* **2021**, *23*, 100535. [CrossRef]
20. Francos, M.; Úbeda, X.; Tort, J.; Panareda, J.M.; Cerdà, A. The Role of Forest Fire Severity on Vegetation Recovery after 18 Years. Implications for Forest Management of *Quercus suber* L. in Iberian Peninsula. *Glob. Planet. Chang.* **2016**, *145*, 11–16. [CrossRef]
21. Vanderhoof, M.K.; Hawbaker, T.J.; Ku, A.; Merriam, K.; Berryman, E.; Cattau, M. Tracking Rates of Postfire Conifer Regeneration vs. Deciduous Vegetation Recovery across the Western United States. *Ecol. Appl.* **2021**, *31*, e02237. [CrossRef]
22. Bright, B.C.; Hudak, A.T.; Kennedy, R.E.; Braaten, J.D.; Henareh Khalyani, A. Examining Post-Fire Vegetation Recovery with Landsat Time Series Analysis in Three Western North American Forest Types. *Fire Ecol.* **2019**, *15*, 8. [CrossRef]
23. Cuevas-González, M.; Gerard, F.; Balzter, H.; Riaño, D. Analysing Forest Recovery after Wildfire Disturbance in Boreal Siberia Using Remotely Sensed Vegetation Indices. *Glob. Chang. Biol.* **2009**, *15*, 561–577. [CrossRef]
24. Tran, B.N.; Tanase, M.A.; Bennett, L.T.; Aponte, C. Evaluation of Spectral Indices for Assessing Fire Severity in Australian Temperate Forests. *Remote Sens.* **2018**, *10*, 1680. [CrossRef]
25. Ramsay, P.M. Giant Rosette Plant Morphology as an Indicator of Recent Fire History in Andean Páramo Grasslands. *Ecol. Indic.* **2014**, *45*, 37–44. [CrossRef]
26. Borrelli, P.; Armenteras, D.; Panagos, P.; Modugno, S.; Schütt, B. The Implications of Fire Management in the Andean Paramo: A Preliminary Assessment Using Satellite Remote Sensing. *Remote Sens.* **2015**, *7*, 11061–11082. [CrossRef]
27. Zomer, M.A.; Ramsay, P.M. Post-fire Changes in Plant Growth Form Composition and Diversity in Andean Páramo Grassland. *Appl. Veg. Sci.* **2021**, *24*, e12554. [CrossRef]
28. Lara, J.G.M.; Mendoza, C.I.Á.; Coronel, L.J.J. Assessment of Fuel Related Data in the Metropolitan District of Quito for Modeling and Simulation of Wildfires, Case Study: Atacazo Hill Wildfire. *Granja* **2022**, *34*, 43–59. [CrossRef]
29. Reyes-Bueno, F.; Loján-Córdova, J. Assessment of Three Machine Learning Techniques with Open-Access Geographic Data for Forest Fire Susceptibility Monitoring—Evidence from Southern Ecuador. *Forests* **2022**, *13*, 474. [CrossRef]
30. Carrión-Paladines, V.; Hinojosa, M.B.; Álvarez, L.J.; Reyes-Bueno, F.; Quezada, L.C.; García-Ruiz, R. Effects of the Severity of Wildfires on Some Physical-Chemical Soil Properties in a Humid Montane Scrublands Ecosystem in Southern Ecuador. *Fire* **2022**, *5*, 66. [CrossRef]
31. Pérez-Cabello, F.; Montorio, R.; Alves, D.B. Remote Sensing Techniques to Assess Post-Fire Vegetation Recovery. *Curr. Opin. Environ. Sci. Health* **2021**, *21*, 100251. [CrossRef]
32. Gobierno Autónomo Descentralizado del Canton Quilanga. Plan de Ordenamiento Territorial Del Cantón Quilanga, Tema: Precipitación. 2014.

33. Alcaldia del Cantón Quilanga Incendio Forestal en Quilanga. Available online: https://www.facebook.com/fredy.cuevarojas.1/videos/145016750072990/ (accessed on 17 October 2021).
34. Keeley, J.E. Fire Intensity, Fire Severity and Burn Severity: A Brief Review and Suggested Usage. *Int. J. Wildland Fire* **2009**, *18*, 116–126. [CrossRef]
35. UN-SPIDER Knowledge Portal Normalized Burn Ratio (NBR). Available online: https://un-spider.org/advisory-support/recommended-practices/recommended-practice-burn-severity/in-detail/normalized-burn-ratio (accessed on 17 October 2021).
36. Mpakairi, K.S.; Ndaimani, H.; Kavhu, B. Exploring the Utility of Sentinel-2 MSI Derived Spectral Indices in Mapping Burned Areas in Different Land-Cover Types. *Sci. Afr.* **2020**, *10*, e00565. [CrossRef]
37. Chen, X.; Vogelmann, J.E.; Rollins, M.; Ohlen, D.; Key, C.H.; Yang, L.; Huang, C.; Shi, H. Detecting Post-Fire Burn Severity and Vegetation Recovery Using Multitemporal Remote Sensing Spectral Indices and Field-Collected Composite Burn Index Data in a Ponderosa Pine Forest. *Int. J. Remote Sens.* **2011**, *32*, 7905–7927. [CrossRef]
38. Efthimiou, N.; Psomiadis, E.; Panagos, P. Fire Severity and Soil Erosion Susceptibility Mapping Using Multi-Temporal Earth Observation Data: The Case of Mati Fatal Wildfire in Eastern Attica, Greece. *Catena* **2020**, *187*, 104320. [CrossRef] [PubMed]
39. Hislop, S.; Jones, S.; Soto-Berelov, M.; Skidmore, A.; Haywood, A.; Nguyen, T.H. Using Landsat Spectral Indices in Time-Series to Assess Wildfire Disturbance and Recovery. *Remote Sens.* **2018**, *10*, 460. [CrossRef]
40. Petropoulos, G.P.; Griffiths, H.M.; Kalivas, D.P. Quantifying Spatial and Temporal Vegetation Recovery Dynamics Following a Wildfire Event in a Mediterranean Landscape Using EO Data and GIS. *Appl. Geogr.* **2014**, *50*, 120–131. [CrossRef]
41. Breiman, L. Random Forests. *Mach. Learn.* **2001**, *45*, 5–32. [CrossRef]
42. Immitzer, M.; Neuwirth, M.; Böck, S.; Brenner, H.; Vuolo, F.; Atzberger, C. Optimal Input Features for Tree Species Classification in Central Europe Based on Multi-Temporal Sentinel-2 Data. *Remote Sens.* **2019**, *11*, 2599. [CrossRef]
43. Romo Leon, J.R.; van Leeuwen, W.J.D.; Casady, G.M. Using MODIS-NDVI for the Modeling of Post-Wildfire Vegetation Response as a Function of Environmental Conditions and Pre-Fire Restoration Treatments. *Remote Sens.* **2012**, *4*, 598–621. [CrossRef]
44. Li, M.; Guo, X. Evaluating Post-Fire Vegetation Recovery in North American Mixed Prairie Using Remote Sensing Approaches. *Open J. Ecol.* **2018**, *8*, 646–680. [CrossRef]
45. Hammill, K.A.; Bradstock, R.A. Remote Sensing of Fire Severity in the Blue Mountains: Influence of Vegetation Type and Inferring Fire Intensity. *Int. J. Wildland Fire* **2006**, *15*, 213–226. [CrossRef]
46. Trigg, S.; Flasse, S. An Evaluation of Different Bi-Spectral Spaces for Discriminating Burned Shrub-Savannah. *Int. J. Remote Sens.* **2001**, *22*, 2641–2647. [CrossRef]
47. Qin, Q.; Xu, D.; Hou, L.; Shen, B.; Xin, X. Comparing Vegetation Indices from Sentinel-2 and Landsat 8 under Different Vegetation Gradients Based on a Controlled Grazing Experiment. *Ecol. Indic.* **2021**, *133*, 108363. [CrossRef]
48. Steiner, J.L.; Wetter, J.; Robertson, S.; Teet, S.; Wang, J.; Wu, X.; Zhou, Y.; Brown, D.; Xiao, X. Grassland Wildfires in the Southern Great Plains: Monitoring Ecological Impacts and Recovery. *Remote Sens.* **2020**, *12*, 619. [CrossRef]
49. Liu, J.; Maeda, E.E.; Wang, D.; Heiskanen, J. Sensitivity of Spectral Indices on Burned Area Detection Using Landsat Time Series in Savannas of Southern Burkina Faso. *Remote Sens.* **2021**, *13*, 2492. [CrossRef]
50. Shahi, K.; Shafri, H.Z.M.; Taherzadeh, E.; Mansor, S.; Muniandy, R. A Novel Spectral Index to Automatically Extract Road Networks from WorldView-2 Satellite Imagery. *Egypt. J. Remote Sens. Space Sci.* **2015**, *18*, 27–33. [CrossRef]
51. Alcaras, E.; Costantino, D.; Guastaferro, F.; Parente, C.; Pepe, M. Normalized Burn Ratio Plus (NBR+): A New Index for Sentinel-2 Imagery. *Remote Sens.* **2022**, *14*, 1727. [CrossRef]
52. Liu, S.; Zheng, Y.; Dalponte, M.; Tong, X. A Novel Fire Index-Based Burned Area Change Detection Approach Using Landsat-8 OLI Data. *Eur. J. Remote Sens.* **2020**, *53*, 104–112. [CrossRef]
53. Caon, L.; Vallejo, V.R.; Coen, R.J.; Geissen, V. Effects of Wildfire on Soil Nutrients in Mediterranean Ecosystems. *Earth Sci. Rev.* **2014**, *139*, 47–58. [CrossRef]
54. White, J.D.; Ryan, K.C.; Key, C.C.; Running, S.W. Remote Sensing of Forest Fire Severity and Vegetation Recovery. *Int. J. Wildland Fire* **1996**, *6*, 125–136. [CrossRef]
55. Asrar, G.; Myneni, R.B.; Li, Y.; Kanemasu, E.T. Measuring and Modeling Spectral Characteristics of a Tallgrass Prairie. *Remote Sens. Environ.* **1989**, *27*, 143–155. [CrossRef]
56. Gordon, C.E.; Price, O.F.; Tasker, E.M. Mapping and Exploring Variation in Post-Fire Vegetation Recovery Following Mixed Severity Wildfire Using Airborne LiDAR. *Ecol. Appl.* **2017**, *27*, 1618–1632. [CrossRef] [PubMed]
57. Maxwald, M.; Crocetti, C.; Ferrari, R.; Petrone, A.; Rauch, H.P.; Preti, F. Soil and Water Bioengineering Applications in Central and South America: A Transferability Analysis. *Sustainability* **2020**, *12*, 10505. [CrossRef]
58. Girona-García, A.; Vieira, D.C.S.; Silva, J.; Fernández, C.; Robichaud, P.R.; Keizer, J.J. Effectiveness of Post-Fire Soil Erosion Mitigation Treatments: A Systematic Review and Meta-Analysis. *Earth Sci. Rev.* **2021**, *217*, 103611. [CrossRef]
59. Zaimes, G.N.; Kasapidis, I.; Gkiatas, G.; Pagonis, G.; Savvopoulou, A.; Iakovoglou, V. Targeted Placement of Soil Erosion Prevention Works after Wildfires. *IOP Conf Ser Earth Environ Sci* **2020**, *612*, 12050. [CrossRef]
60. Bandy, D.; Garrity, D.P.; Sánchez, P. EL Problema Mundial de La Agricultura de Tala y Quema. *Agroforestería Américas* **1994**, *1*, 14–20.
61. Armenteras, D.; González, T.M.; Ríos, O.V.; Elizalde, M.C.M.; Oliveras, I. Fire in the Ecosystems of Northern South America: Advances in the Ecology of Tropical Fires in Colombia, Ecuador and Peru. *Caldasia* **2020**, *42*, 1–16. [CrossRef]

62. Copernicus Climate Change Service Fire Weather Index. Available online: https://climate.copernicus.eu/fire-weather-index (accessed on 21 June 2022).
63. Datt, B. A New Reflectance Index for Remote Sensing of Chlorophyll Content in Higher Plants: Tests Using Eucalyptus Leaves. *J. Plant Physiol.* **1999**, *154*, 30–36. [CrossRef]
64. Pinty, B.; Verstraete, M.M. GEMI: A Non-Linear Index to Monitor Global Vegetation from Satellites. *Vegetatio* **1992**, *101*, 15–20. [CrossRef]
65. le Maire, G.; François, C.; Dufrêne, E. Towards Universal Broad Leaf Chlorophyll Indices Using PROSPECT Simulated Database and Hyperspectral Reflectance Measurements. *Remote Sens. Environ.* **2004**, *89*, 1–28. [CrossRef]
66. Gitelson, A.A.; Kaufman, Y.J.; Merzlyak, M.N. Use of a Green Channel in Remote Sensing of Global Vegetation from EOS-MODIS. *Remote Sens. Environ.* **1996**, *58*, 289–298. [CrossRef]
67. Wulf, H.; Stuhler, S. Sentinel-2: Land Cover, Preliminary User Feedback on Sentinel-2A Data. In Proceedings of the Sentinel-2A Expert Users Technical Meeting, Frascati, Italy, 29–30 September 2015; pp. 29–30.
68. Radoux, J.; Chomé, G.; Jacques, D.C.; Waldner, F.; Bellemans, N.; Matton, N.; Lamarche, C.; D'Andrimont, R.; Defourny, P. Sentinel-2's Potential for Sub-Pixel Landscape Feature Detection. *Remote Sens.* **2016**, *8*, 488. [CrossRef]
69. Tucker, C.J. Red and Photographic Infrared Linear Combinations for Monitoring Vegetation. *Remote Sens Environ* **1979**, *8*, 127–150. [CrossRef]
70. Filella, I.; Peñuelas, J. The Red Edge Position and Shape as Indicators of Plant Chlorophyll Content, Biomass and Hydric Status. *Int. J. Remote Sens.* **1994**, *15*, 1459–1470. [CrossRef]
71. Chen, P.; Tremblay, N.; Wang, J.; Vigneault, P.; Huang, W.; Li, B. New Index for Crop Canopy Fresh Biomass Estimation. *Spectrosc. Spectr. Anal.* **2010**, *30*, 512–517.
72. Lichtenthaler, H.K.; Lang, M.; Sowinska, M.; Heisel, F.; Miehé, J.A. Detection of Vegetation Stress via a New High Resolution Fluorescence Imaging System. *J. Plant Physiol.* **1996**, *148*, 599–612. [CrossRef]
73. Alan Blackburn, G. Quantifying Chlorophylls and Caroteniods at Leaf and Canopy Scales: An Evaluation of Some Hyperspectral Approaches. *Remote Sens. Environ.* **1998**, *66*, 273–285. [CrossRef]
74. Domenech, E.; Mallet, C. Change Detection in High-Resolution Land Use/Land Cover Geodatabases (At Object Level). In *European Spatial Data Research*; EuroSDR: Vienna, Austria, 2014; Volume 64, pp. 9–57.